Fe on Au(001): magnetism and band formation

1993 J. Phys.: Condens. Matter 5 4647

(http://iopscience.iop.org/0953-8984/5/27/010)

J. Phys.: Condens. Matter 5 (1993) 4647–4664. Printed in the UK

Fe on Au(001): magnetism and band formation

S Crampin

Institute for Theoretical Physics, Catholic University of Nijmegen, Toernooiveld, NL-6525 ED Nijmegen, The Netherlands

Received 12 February 1993

Abstract. The development of thin-film electronic and magnetic properties with film size are addressed in a study of Fe on Au(001), up to 10 Fe layers thick and including the Au overlayer formed during normal growth conditions. Enhanced moments at the Fe/Au interface are observed, decaying to bulk over 3 Fe layers, and the weak Fe–Au interaction is reflected in moments similar to those of the Fe(001) surface and in a very small asymmetry in the magnetic properties of the Fe film. Calculated hyperfine fields are found to exhibit a strong dependence upon film thickness and no simple relationship with the local spin moments. Densities of states and core-level shifts reflect changes in nearest-neighbour species and give a consistent picture of the interface bonding. The development of zone-centre states with film thickness is followed, and bulk-band overlap and interfacial bonding are found to influence the distribution of quantum well states strongly.

1. Introduction

New techniques in crystal growth have enabled the preparation of high-quality magnetic thin-film and overlayer structures, prompting much fundamental and technologically orientated research. Part of this interest arises from the opportunity to test our understanding of magnetic behaviour and our ability to model it, generating strong interplay between experimental, theoretical and computational physics. Studies of γ-Fe grown on Cu(001) (Bader and Moog 1987, Fu and Freeman 1987) and ϵ-Fe in FeRu multilayers (Maurer *et al* 1991, Knab and Koenig 1991) are cases to hand. Partly, the interest stems from potential applications in magnetic recording devices, exploiting novel behaviour such as giant magnetoresitivity (Shinto *et al* 1990) or reduced Curie temperatures.

This article describes a study on the Fe/Au(100) system. Noble metal substrates have found favour in numerous experimental and theoretical studies. The low d band of the noble metal keeps hybridization effects to a minimum and thus allows a partial realization of the unattainable isolated magnetic-film system, and thus the study of quasi-two-dimensional magnetism. For several substrate orientations and overlayer species only small lattice mismatches are present, which encourages the formation of sharp interfaces. The energy region between the Fermi energy and the top of the substrate metal d band (at 2 eV, 3.5 eV and 2.5 eV binding energy for Cu, Ag and Au respectively) also provides weak sp emission in photoemission, a suitable backdrop against which to study the formation of the overlayer band structure. The occupied and unoccupied states of Fe/Au have both been studied experimentally (Heinen *et al* 1990, Himpsel 1991). In addition, the Fe/Au system has been studied with regard to thin-film Curie temperatures (Bader *et al* 1986), and exhibits a magnetic phase transition with an anomolous order parameter (Dürr *et al* 1989).

0953-8984/93/274647+18$07.50

Fe/Au films have been used to study exchange coupling across non-magnetic spacer layers (Fuss *et al* 1992).

The Fe/Au(100) system is particularly well lattice matched, the square surface mesh of the substrate (side: $a/\sqrt{2} = 2.88$ Å) and the (100) net of bulk Fe ($a = 2.87$ Å) differing by only 0.5%. Consequently, 1×1 growth of BCC Fe is expected. Low-energy electron diffraction spectra indicate that deposition of ~ 0.2 monolayers of Fe causes reversion of the clean 5×20 Au reconstruction to a 1×1 structure (Bader and Moog 1987, Himpsel 1991), which then persists for greater Fe coverages. Growth proceeds layer by layer, with no evidence for a maximum stable film thickness associated with the formation of metastable γ-Fe. Auger electron spectroscopy during growth and on sputtered Fe/Au(100) surfaces reveals the presence of a single Au monolayer capping the Fe film (Bader and Moog 1987), the relatively low surface energy of Au (liquid surface tensions 1100 erg cm^{-2} (Au) versus 1900 (Fe) erg cm^{-2}) promoting the retention of the Au at the surface during growth. The existence of the Au overlayer is confirmed by image-state measurements (Himpsel 1991) finding the $n = 1$ image state close to that of Au(100) (falling by ~ 0.3 eV with the deposition of the first monolayer and then constant). The image state, trapped in the long-range tail of the vacuum potential, is primarily sensitive to the value of the work function (Hölzl and Schulte 1979: Au = 5.5 eV, Fe = 4.7 eV) and secondarily to the crystal electronic structure.

In this work the magnetic and electronic properties of the Fe/Au(001) system are investigated, giving particular attention to the range over which interfacial features persist in thicker films and to the development of the electron states. Parameter-free self-consistent electronic structure calculations have been performed for a monolayer, bilayer, trilayer etc up to Fe film thicknesses of ten layers, each capped by a single Au layer on the vacuum surface and coupled to a semi-infinite Au(001), for which three Au planes at the Fe/Au interface are treated self-consistently. For reference, the electronic structure of a clean (hypothetical) 1×1 Au(001) surface has also been evaluated, some Fe monolayers buried by 2–4 Au layers, and AuFeAu sandwiches. It is inevitable in a study such as this that approximations must be made for a tractable solution, and the method of calculation is discussed in the following section. Subsequent sections describe the development of work functions, core level shifts, magnetic moments and electronic states as functions of Fe thickness.

2. Tools of the trade

These calculations have been performed within the local density approximation with the multiple-scattering layer Korringa–Kohn–Rostoker (LKKR) electronic structure method, which has been described by MacLaren and co-workers (1989). This method is a generalization to two-dimensional translational symmetry of conventional KKR theory. It is capable of reproducing all bulk KKR results, with the additional ability to study interfacial systems. The site-diagonal scattering path operator τ entering the usual expression for the one-electron Green function is obtained from a two-dimensional Brillouin zone integral

$$\tau_\nu = \int_\Omega \frac{\mathrm{d}\boldsymbol{k}_\parallel}{\Omega} \left[t_\nu^{-1} - \mathrm{g}_\nu(\boldsymbol{k}_\parallel) - \Delta_\nu(\boldsymbol{k}_\parallel)\right]^{-1} \tag{1}$$

where t is the atomic scattering t matrix, $g(\boldsymbol{k}_\parallel)$ an intralayer propagator and $\Delta(\boldsymbol{k}_\parallel)$ a propagator summing scattering paths external to the layer ν (Crampin *et al* 1990). Partitioning the scattering paths in this manner allows the use of layer scattering algorithms

which dispense with reciprocal space normal to the layers. These algorithms sum scattering paths at a linear rate within dissimilar layers and an exponential rate for identical layers, leading to an efficient computational scheme whilst dispensing with artificial devices such as slabs and supercells and their associated deficiencies. In particular, there is no artificial surface–surface interaction and the continuum of states is correctly realized.

Recently, Skriver and Rosengaard (1991) have demonstrated the validity of the atomic sphere approximation for surface calculations, including the representation of the vacuum potential by so-called 'empty spheres' (in the sense of containing no nuclear charge). This approximation is used here. The essential ingredient in this approach is the inclusion of dipole contributions from the atom-centred charge distribution in the solution of the Poisson equation, which is necessary to generate a correct description of the surface dipole barrier and to describe the potential shift across interfacial planes. The successful description of the vacuum potential, which rises rapidly over 1–2 Å outside the crystal, is rather surprising. In fact, what would appear to be a more appropriate description, that of a z-dependent barrier potential, turns out to be less successful (Crampin 1992). The implementation of such a potential is relatively simple within the LKKR framework, with the Green function in the vacuum region expanded in solutions of the one-dimensional Schrödinger equation for the barrier which also give the barrier reflectivity necessary to sum the multiple scattering paths. However, work functions are typically a half to one volt worse than those obtained with the atomic sphere representation, an error which apparently originates in the double counting of volume at the solid–vacuum interface. Space-filling atomic spheres overlap along nearest-neighbour directions whilst some interstitial volume is external to the spheres. A z-dependent barrier potential must approach to within half an interplanar spacing (neglecting relaxation) of the surface layer to be space filling. The ratio of double-counted volume between the surface layer and the vacuum potential in the case of the atomic sphere representation and the barrier potential representation is 1:1.18 for FCC(111) and 1:1.62 for FCC(001), becoming worse for more open surfaces. The z-dependent barrier is in worse error exactly from where the major contribution to the work function arises, basically because the atomic spheres overlap in plane as well as across planes. Note that a more accurate implementation of a z-dependent barrier potential might be achieved by Green-function matching over the surface of the atomic spheres, as has been done in the case of a constant vacuum potential by Inglesfield (1978). The success of the atomic sphere representation of the vacuum potential seems to make this development unnecessary, although it might need to be invoked for more open surfaces.

The use of the atomic sphere approximation introduces errors into the scattering treatment (strictly valid only for non-overlapping potentials) but this is more than compensated for by the improved description of the crystal potential. This has been recognized in other defect calculations (see, e.g., Drittler *et al* 1989) and is one of the benefits of the LMTO/ASW methods. At the surface the atomic sphere representation is particularly beneficial in making the interstitial region effectively redundant, reducing it to nothing more than an expansion device. If one were to persist with the muffin-tin representation it would be necessary to use a z-dependent muffin-tin zero (average interstitial potential) in order to adequately describe the potential variation. This could most easily be accomplished by a layer-dependent constant, but the scattering treatment—whilst not intractable—would be significantly more complicated.

The solution of the Poisson equation employed here differs slightly from that of Skriver and Rosengaard (1991) in that charge neutrality is not imposed directly. Rather, the Au substrate is used as a source of electrons which are allowed to flow freely in and out of the surface region. This recognizes the fact that there are long-range oscillations within the

charge density (Friedel oscillations) which result in deviations from neutrality up to arbitrary distances from the surface. In practice, results depend little upon whether charge neutrality has been imposed or not, although the present scheme can also accommodate an electric field at the surface. In the calculations presented here deviations from local neutrality (i.e. within the volume treated self-consistently) were never more than 0.001 electrons, whilst the valence charge treated self-consistently was up to 124 electrons. The Poisson equation is solved with zero derivative boundary condition outside the surface (midway between the second and third (non-existent) layer of vacuum spheres) and continuity with the bulk potential on the plane midway between the third and fourth Au layers entering the substrate.

The structure was modelled as follows. The in-plane dimension was fixed at that of the Au substrate ($a = 4.078/\sqrt{2}$ Å) and interplanar spacings taken to be those generated by touching spheres of bulk radii. In all cases possible relaxation at the surface was neglected. It seems reasonable to expect that, compared to bulk Fe, the increased in-plane spacing is accompanied by a reduced normal spacing, even within the thicker films (as seen e.g. in Co/Cu(001)). Because of the good lattice match any uncertainty will only have a marginal effect on calculated properties (the resulting Fe volume per atom within the thicker films is only 1% smaller than that in bulk Fe). The calculation included partial waves up to $\ell = 2$ and intermediate expansions of the scattering paths performed in the energy-dependent plane-wave basis using 25 g vectors. Ideally $\ell = 3$ should be used, but this obviously gives rise to a significant increase in calculation times. The effects of truncation at $\ell = 2$ are commented upon below. Valence band integrals in evaluating the charge density were performed by 16-point Gaussian quadrature over a semi-circular contour in the upper half of the complex plane—this is very accurate. Brillouin-zone integrations were performed by special points (ten points in the 1/8th irreducible zone). Relativistic effects were incorporated within the scalar-relativistic approximation of Koelling and Harmon (1977) for both core and valence states, keeping spin as a good quantum number by neglecting spin–orbit coupling but incorporating the mass-velocity, Darwin and higher-order terms. This is not expected to affect calculated moments, work functions or core level shifts greatly, but will affect single-particle spectra. The local spin-density approximation is used in the form of von Barth and Hedin (1972) with the parametrization of Moruzzi *et al* (1978). In evaluating the local density of states, 136 special points in the 1/8th irreducible zone were used, and a straight-line contour displaced by 0.1 eV above the real energy axis.

In the following, the Au layers entering the solid are referred to as Au(1), Au(2) and Au(3). The Au overlayer is simply referred to as Au, and the Fe layers Fe(1), Fe(2), to Fe(n), with Fe(n) the layer at the interface with the Au substrate, touching Au(1). For the clean Au surface, the overlayer is omitted.

3. Au(001)

For reference the ideal Au(001)–1 × 1 surface was treated self-consistently with the one-electron potential of the top 3 layers + 2 vacuum layers allowed to relax. The calculated work function $\Phi = 5.44$ eV agrees well with experimentally determined values of $\Phi = 5.47$ eV (Hölzl and Schulte 1979) and 5.22 eV (Hansson and Flodström 1978). Note that whereas the actual Au(001)–5 × 20 surface might be expected to show a rather different work function than Au(001)–1 × 1, from the usual arguments of double-layer formation at rougher surfaces, there appears to be little variation of Φ over the principal crystal faces (Hölzl and Schulte 1979, Hansson and Flodström 1978) and only ~ 0.1–0.2 eV variations on various stepped surfaces (Besocke *et al* 1977). As a caveat, the work function arises

from a region of the crystal where the electron density varies rapidly so the calculated work function is rather sensitive to the particular choice of the exchange–correlation functional (Skriver and Rosengaard 1991).

In figure 1 the layer projected local density of states is shown. The bulk profile is already reasonably well recovered within the Au(3) atom, three layers from the surface. The surface atom exhibits band narrowing (in the sense of the root mean square width, rather than the full band width which is unaltered) as expected from the reduction in nearest neighbours. This narrowing is asymmetric, the top of the d band lining up with the bulk d band maximum (at 2 eV binding energy) with the width reduction occurring in the low energy region from 6–8 eV binding energy. This may be viewed as a two-step process, the reduction in nearest neighbours narrowing the band and a rise in the surface potential re-aligning the d band maxima. The surface core-level shift, which measures the rise in surface potential, is found to be +0.43 eV, in good agreement with the experimental shift of $+0.40 \pm 0.01$ eV (Citrin *et al* 1978). This rise in surface potential is clearly visible in figure 1 as a rise of ~ 0.5 eV of the 5s valence band (up from a binding energy of 7.3 eV on the bulk sites) and the Au d levels—this is also in good agreement with the 0.51 ± 0.08 eV deduced from x-ray photoemission (Citrin *et al* 1978).

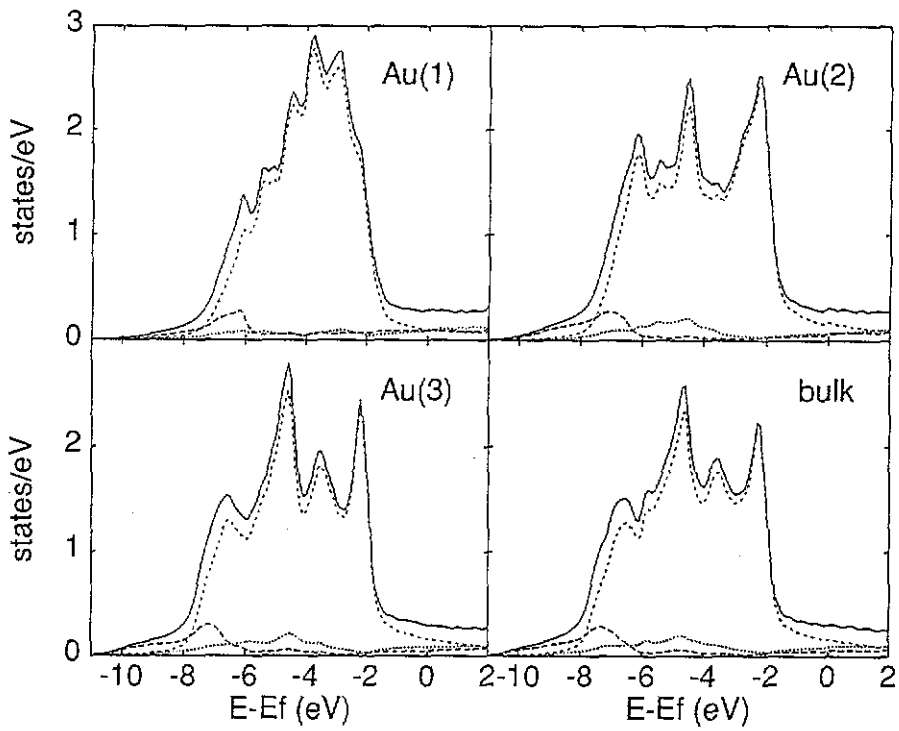

Figure 1. Layer-resolved atomic-sphere densities of states for the Au(100)–1 × 1 surface. Au(1) is the surface atom, Au(2) the sub-surface atom and Au(3) the atom in the third layer down. Full curve—total density of states. Long/medium/short dash—s/d/p contributions.

4. Au/Fe/Au(001)

The introduction of a single monolayer of Fe ($Au_1Fe_1Au_\infty$) is found to reduce the work function to 4.95 eV, with subsequent Fe layers stabilizing Φ at 5.05 eV. Himpsel (1991) has presented data indicating a drop of some 0.3 eV in the $n = 1$ image state upon completion of the first Fe monolayer, which then remains approximately constant. The present calculation does not include the coulombic tail of the exact exchange–correlation potential, a feature beyond the local-density approximation, and hence the hydrogenic sequence of image states is not reproduced. However, the local density barrier is sufficiently strong to localize a surface state, the weight of which is predominantly within the outermost vacuum sphere (the relative weight beyond this volume has not been determined). This is the local-density analogue of the $n = 1$ image state, and the calculations indicate a drop from 4.85 eV on the clean Au(001)–1 × 1 surface to around 4.5 eV for the thicker Fe overlayer films.

Table 1. Calculated atomic-sphere spin moments (in μ_B) for the $Au_1Fe_nAu_\infty$ overlayer system. The moment of Au(3) was always $0.00\mu_B$.

n	Au}	Fe(1)...	Fe(n)}	Au(1)	Au(2)								
1	0.04}	3.01}	0.01	−0.01									
2	0.04}	2.85	2.76}	0.05	0.00								
3	0.05}	2.84	2.47	2.77}	0.04	0.00							
4	0.05}	2.85	2.50	2.44	2.80}	0.04	−0.01						
5	0.06}	2.83	2.43	2.35	2.41	2.78}	0.04	−0.01					
6	0.06}	2.85	2.45	2.36	2.42	2.41	2.81}	0.05	0.00				
7	0.06}	2.83	2.43	2.28	2.32	2.33	2.42	2.79}	0.05	0.00			
8	0.06}	2.84	2.43	2.29	2.29	2.27	2.36	2.39	2.79}	0.04	0.00		
9	0.06}	2.83	2.41	2.26	2.28	2.22	2.27	2.31	2.38	2.78}	0.04	0.00	
10	0.06}	2.83	2.41	2.26	2.27	2.23	2.25	2.24	2.33	2.38	2.78}	0.04	0.00

The local spin moments at each site are found by integrating the magnetization density over the volume of the atomic sphere. The results are presented in table 1. The moments themselves are converged to better than $0.001\mu_B$, although numerical approximations (basis set truncation, Brillouin zone integration, etc) introduce a systematic error of the order of $+0.05\mu_B$, estimated from various calculations improving these approximations for bulk Fe and some smaller Fe/Au systems. There is an additional intrinsic error arising from the use of the local spin-density theory, and even within this approximation various explicit forms for the local spin-density potential give rise to moments which can differ by some 5%. The *relative* behaviour of the moments in table 1 is more stable than this though.

Within the Fe monolayer, each atom is surrounded by four other Fe atoms at a separation corresponding to the second-nearest-neighbour spacing within bulk Fe. This results in strong band narrowing and a consequent enhancement of the magnetism, with the monolayer Fe exhibiting a moment of $3.01\mu_B$, enhanced by over 30% above the bulk moment. Note that burying the monolayer by further Au overlayers has only a small effect on the moment—falling to 2.98, 2.94 and $2.94\mu_B$ with 2, 3 and 4 Au layers respectively. The Fe bilayer introduces neighbours at bulk nearest-neighbour separations—each Fe atom has one half of the bulk complement of eight nearest neighbours. Consequently, the moment on the Fe(1) site falls to $2.85\mu_B$, which still represents an enhancement of 25% over the bulk value, and this value changes little with the addition of subsequent Fe layers. At the Fe/Au–substrate interface, the Fe(n) moment is $2.76\mu_B$ for $n = 2$ and $2.78\mu_B$ in the case of $n = 10$, the

asymmetry in the thin-film environment being constantly reflected in a marginally smaller moment (by 0.05–0.10μ_B) on the substrate side of the Fe film. This smaller moment reflects the greater band width of the Au(1) layer relative to the Au overlayer, whilst the size of the asymmetry reveals the minor role of Fe–Au hybridization, due to the d band misalignment.

The moment on the Fe layers within the film is generally enhanced over bulk for thin films, whilst for the thicker films the moment falls to the bulk value over 2–3 layers. The enhanced moments reflect decreased band widths within the thin films. There are some small fluctuations in the layer moments within the thicker films which are probably artificial, arising from incomplete Brillouin zone integration. Individual states are significantly affected by the presence of an interface and it is only when one sums over a large number that the phase information interferes destructively and the influence of the interface decays over a screening length. There still remain long-range effects, Friedel oscillations, and it is possible that there give rise to the fluctuation moments. Nevertheless, the fluctuations are small, a few hundredths of a μ_B. An FLAPW study of the Fe(001) surface using a seven-layer slab gave moments of 2.98, 2.35, 2.39 and 2.25μ_B (Ohnishi *et al* 1983) whilst a tight-binding study omitting sp electrons gave 2.60, 2.17, 2.16 and 2.18μ_B for a similar seven-layer slab (Mokrani *et al* 1990). The more stable moments in the latter also tend to suggest that the longer-range sp electrons do give rise to small fluctuations in moments. Interestingly, results for five-layer Fe (001) films studied by Ohnishi and co-workers (1984) exhibited a large oscillation in the layer-by-layer moment, which was removed by Ag overlayers. The results reported here indicate that Au also inhibits this oscillatory behaviour.

Freeman and co-workers have studied other related systems. Li *et al* (1988) considered a five-layer Au(001) slab with Fe monolayers on each surface ($Fe_1Au_5Fe_1$), obtaining an Fe moment of 2.97μ_B. This is very close to the value reported here, 3.01μ_B, for the $Au_1Fe_1Au_\infty$ monolayer and also to the value for a free-standing (001) Fe monolayer, 3.18μ_B, reported by Ohnishi, Weinert and Freeman (1984). This further highlights the weak influence of Fe–Au hybridization on the magnetic moment. Experimentally, direct measurement of surface/overlayer local moments is not possible, although enhanced exchange splittings in surface states seen by photoemission and inverse photoemission give indirect evidence. Recent work has also demonstrated the utility of *in situ* conversion-electron Mössbauer spectroscopy as a probe of surface and interface magnetic properties (Korecki and Gradmann 1985), although non-proportionality between hyperfine fields and magnetic moments complicates the interpretation (Freeman and Fu 1987). The primary contribution to the hyperfine field, the Fermi contact term, has been determined for the systems studied. The findings are summarized as follows:

(1) For Fe atoms in all the film overlayers, the core contribution scales with the spin moment (-133 ± 1 kG/μ_B). The exchange interaction is attractive between electrons of like spin and hence the net core density at the nucleus depends upon the relative distribution of s core wavefunctions and the radial magnetization density, $m(r)$. Both 1s and 2s electrons lie within $m(r)$, resulting in a negative polarization at the nucleus, the 1s contribution being small due to small overlap with $m(r)$. The 3s wavefunction is largely outside $m(r)$ and gives a positive polarization at the nucleus, somewhat smaller than the 2s contribution. The proportionality between moment and core contribution to the hyperfine field implies that the distribution of the magnetization density is almost independent of environment, which is borne out by comparison of $m(r)$ for various Fe atoms in different film thicknesses. The same holds for $m(r)$ calculated in e.g. bulk BCC Fe, high-spin ferromagnetic and anti-ferromagnetic states of FCC and HCP Fe, and Fe in FeRu alloys and multilayers.

(2) For films of thickness $n \geq 3$, the valence electron contribution at the Fe/Au interface

is *positive* (Fe(n) $\simeq +30$ kG; Fe(1) $\simeq +20$ kG). This results in a total Fermi contact term little changed from bulk. For $n \geqslant 4$ the adjacent Fe atoms (Fe(2), Fe($n-1$)) exhibit an enhanced *negative* conduction electron contribution ($\simeq -60$ kG) and a correspondingly enhanced contact field. Values for other Fe atoms are within ~ 10 kG of bulk values, which are the layer–layer variations in the centre of the largest films. Thus experiments on thicker films of Fe on Au(001) should see an enhanced hyperfine field arising from Fe atoms one layer removed from the interface, whilst the interface atoms which have a larger moment are largely indistinguishable from those at the film centre (within the accuracy of these calculations).

(3) A strong thin-film effect is evident. The monolayer has a large positive valence contribution of $+120$ kG whilst the bilayer Fe atoms show a negative valence contribution of -30 kG. In the trilayer, the central Fe layer has a large negative valence contribution of -80 kG. This suggests that the growth behaviour of Fe on Au can be monitored by hyperfine field measurements.

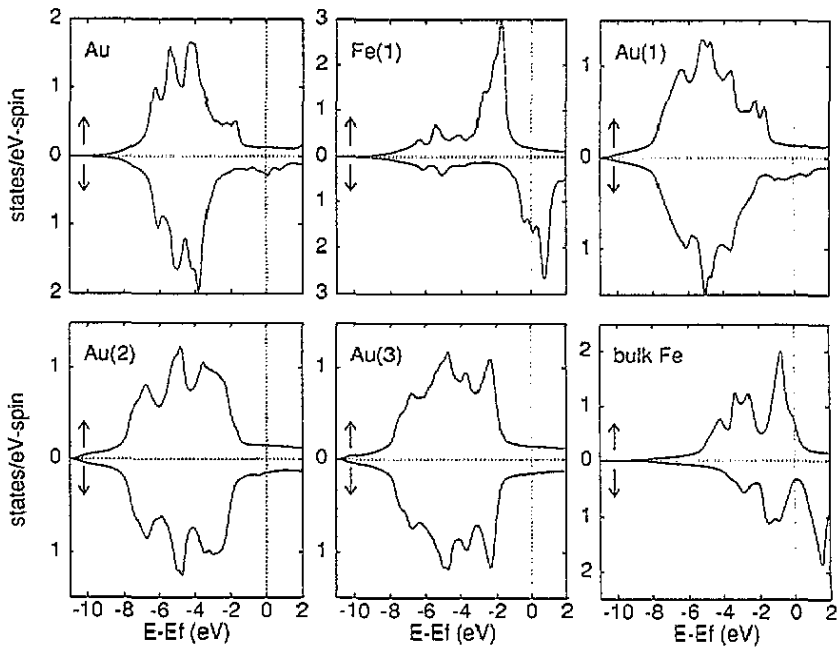

Figure 2. Layer-resolved atomic-sphere densities of states for the $Au_1Fe_1Au_\infty$ system, shown spin resolved. Also shown, bottom right, is the bulk Fe density of states. Note that different vertical scales have been used within the separate panels.

5. Densities of states

The layer-projected densities of states (DOS) for the $Au_1Fe_1Au_\infty$ system are shown in figure 2. The Fe majority d band is fully occupied (strong ferromagnetism) and the Fermi energy lies just below the centre of the minority d band. The spin-splitting of the d band

is approximately 2.5 eV, rather less than might be expected on the basis of a 1 eV/μ_B rough approximation which holds for bulk Fe, Co and Ni. The profile and band width are in rather good agreement with the isolated monolayer DOS shown by Noffke and Fritsche (1981), again highlighting the small Fe–Au interaction, although unlike in the isolated monolayer, the valence band minima are not spin split in this calculation since the s states can hybridize with the Au s states and hence the valence band width is governed by that of the Au substrate which has the same band minimum for both spin directions. This is also the reason why the minority Fe 4s states do not form a separate band which can be seen in the isolated monolayer results of Noffke and Fritsche. Comparing the results in figure 2 with the Fe/Au(100) overlayer calculation of Li and co-workers (1988), the latter does not exhibit the large peak at the top of the majority Fe d band, although they find dispersionless surface states at the relevant energies.

The Au core-level shifts in this system are calculated to be a shift of 0.1 eV on the overlayer and 0.4 eV on the Au(1) site at the Fe/Au interface, both *to greater binding energy*. The full-potential $Fe_1Au_5Fe_1$ calculation of Li and co-workers (1988) also found a downward shift of 0.4 eV on the Au site neighbouring the Fe overlayer. Evidently, the effect of the neighbouring Fe atom is to lower the Au potential (and states), with the overlayer Au atoms also experiencing a competing rise in potential due to the surface effect mentioned previously for the clean Au surface. The Au densities of states are generally consistent with this picture. The Au(1) spin-down band is narrower than bulk Au and lower in energy (the lower d band edges line up well when plotted together), and the same is true for the spin-up band, although a small band of states in the 2–3 eV range, resonant with the Fe monolayer majority d states, make the band width appear greater. The corresponding resonant band does exist upon the minority states, but is a weaker feature due to the greater separation of the Fe and Au spin-down d bands. The overlayer band is considerably narrowed relative to bulk Au, with the band centre coinciding with the bulk band centre. The Au overlayer DOS also exhibits the resonant majority band, and the valence band is characterized by a three-peak structure, due to splittings in the d_{z^2} and d_{xz}, d_{yz} contributions. The layer-resolved Au substrate DOSs are comparable with those of Li and co-workers (1988). The Au(2) layer (12 nearest neighbours) has recovered the bulk band width, has a small spin asymmetry, and on the Au(3) plane the DOS shows the features of bulk Au.

The Fe DOS in the $Au_1Fe_2Au_\infty$ system is greatly different from that in the monolayer case (figure 3), as would be expected from the introduction of four Fe atoms at bulk nearest-neighbour distances, whilst that of the surrounding Au atoms is less affected and indeed shows essentially no change with the introduction of further Fe layers. The Au overlayer core shift remains at 0.1–0.15 eV for all systems studied, whilst the Au(1) shift increases to 0.5 eV for $n = 2$ at which it remains for thicker Fe films, again consistent with the DOS perturbation. Particularly noticeable in the DOS for all the film thicknesses is the symmetry in the profiles for Fe planes equidistant from the Au–overlayer and Au–substrate interfaces, indicating that even a single Au layer acts very much like an Au substrate. This may be seen in figure 4, where Fe(1) and Fe(n) are very similar for film thicknesses $n = 3$ and $n = 4$, as are Fe(2) and Fe(3) for $n = 4$. Figure 4 also illustrates that the bulk DOS profile is largely recovered once the full complement of nearest-neighbour Fe atoms is obtained, which is the case for the central Fe atom in the $n = 3$ film. For $n > 4$ the DOSs at the interface Fe sites are similar to those of Fe(1) and Fe(4) in the $n = 4$ film, and the central sites are bulk like. The Fe core level shift (relative to the central site in the $n = 10$ film) is confined to the interfacial layers (others < 0.05 eV); with the exception of $n = 1$ the shift is 0.6 eV to greater binding energy. For $n = 1$ it is 0.9 eV.

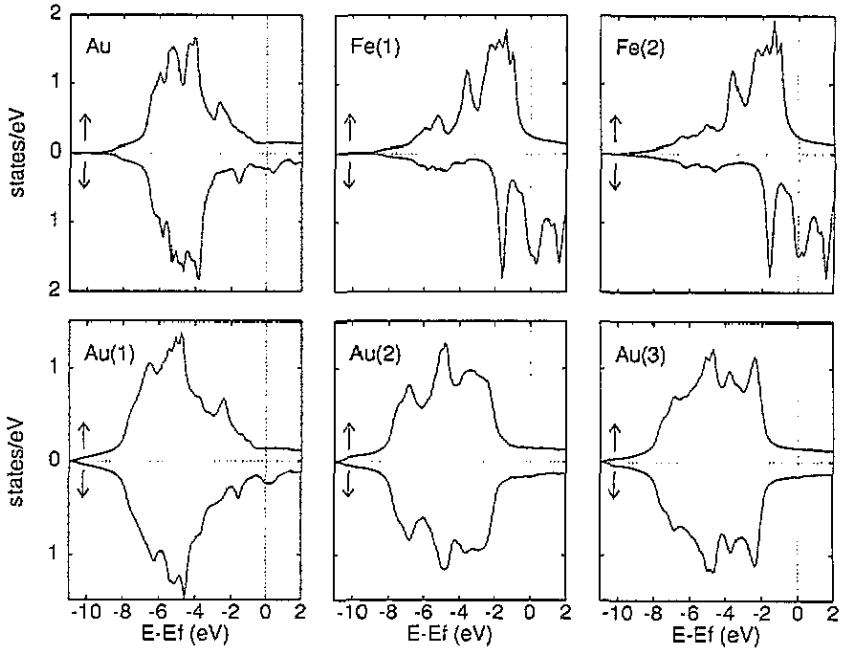

Figure 3. Layer-resolved atomic-sphere densities of states for the $Au_1Fe_2Au_\infty$ system, shown spin resolved.

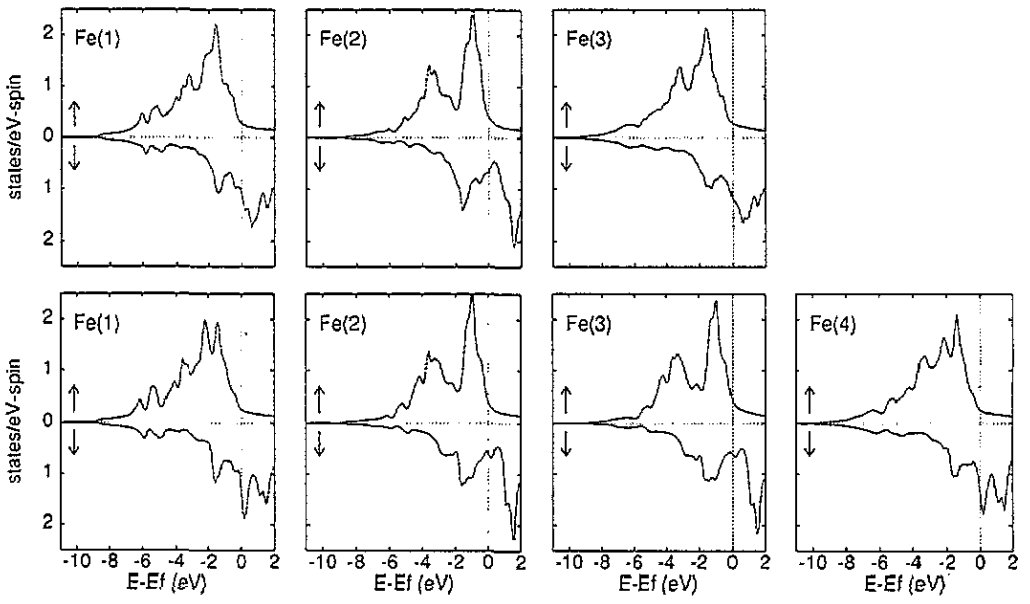

Figure 4. Layer-resolved atomic-sphere densities of states on the Fe layers with the $Au_1Fe_3Au_\infty$ (upper row) and $Au_1Fe_4Au_\infty$ (lower row) system. The Au densities of states are essentially unchanged from those in figure 3.

6. Band formation

In this section the behaviour of the layer-projected DOS at the zone centre of the surface Brillouin zone is examined. In this semi-relativistic calculation the Au single-particle spectra can only be viewed as approximate, since spin–orbit effects are significant. However, relatively few studies of the surface DOS exist which incorporate the true continuum of substrate levels, and so some general features are explored here. The significance of these studies is heightened by recent suggestions regarding the role of localized states in metallic superlattices giving rise to oscillatory exchange couplings (Ortega and Himpsel, 1992). Attention is focused upon zone-centre states, which have received some attention from recent photoemission and inverse photoemission experiments (Heinen *et al* 1990, Himpsel 1991). Whilst being illustrative of the general behaviour to be found in this system, the analysis is considerably simplified by the additional symmetry.

At $\bar{\Gamma}$ the scalar-relativistic states may be labelled according to the irreducible representations of the C_{4v} group, that is Δ_1 (comprising s, p_z and d_{z^2} states), Δ_2 ($d_{x^2-y^2}$), $\Delta_{2'}$ (d_{xy}) and Δ_5 (p_x, p_y, d_{xz} and d_{yz}). Figure 5 shows the results of projecting out the number of electrons within each layer which transform according to these representations for Au(001)–1 × 1. In the −11 to +6 eV energy range, the Δ_2, $\Delta_{2'}$ and Δ_5 states each give rise to a single band, which in the bulk has a characteristic one-dimensional tight-binding (TB) profile. This gives the key to understanding the surface behaviour of these states, for also shown in figure 5(*e*) are the site-resolved DOS $\rho_n(E)$ for a semi-infinite one-band TB linear chain,

$$\rho_n(E) = \sin^2 n\Theta/\pi V \sin\Theta \qquad \Theta = \cos^{-1}[(E - E_A)/2V] \tag{2}$$

where E_A is the on-site energy and V the nearest-neighbour hopping term (see appendix). Clearly, the structure seen in figures 5(*b*)–(*d*) for the surface layers is primarily due to the change in boundary conditions at the metal surface. The states of Δ_1 symmetry are rather more complicated, with three separate bands in the same energy range. Hybridization between these bands results in more complicated dispersion behaviour (to be seen in the bulk band structure) and this is reflected in the DOS profiles. Between 3.5 and 4.5 eV binding energy, for example, the bulk bands are doubled up and give rise to a large peak in figure 5(*a*). At the surface the Δ_1 states couple strongly to the surface potential, as may be expected from symmetry. The calculations indicate a surface state above the lowest band, at −7.0 eV, which decays rapidly into the solid. The corresponding state of Cu(001) has been seen in several calculations. A surface state also exists at an energy of 1.2 eV, which decays more slowly, having sizable weight on the Au(3) layer. Recent inverse photoemission work (Himpsel and Ortega 1992) on the Au–1 × 1 surface has identified a feature at +1.5 eV which is interpreted as an $n = 0$ resonance, with an upper limit of +2.3 eV placed upon the $X_{4'}$ band edge. This indicates a deficiency in the description of the bulk Au band structure, which may be largely due to the semi-relativistic approximation, since another semi-relativistic calculation also places the $X_{4'}$ level well below +2.3 eV (+1 eV according to Jepson *et al* 1981) whilst a calculation by Eckardt and co-workers (1984) including spin–orbit coupling places the corresponding X_{6^+} level about +0.8 eV higher (although this is still low compared to experiment). The omission of $\ell = 3$ scattering may well give rise to a systematic downward shift in the Au bands since including the $\ell = 3$ channel would give rise to approximately 0.06 additional electrons, which would place the Fermi energy lower down on the spd scale.

Consider the behaviour of the DOS in the $Au_1Fe_nAu_\infty$ system. For large n the Fe states will resemble those of bulk Fe, since the Fe and Au lattice parameters are so well

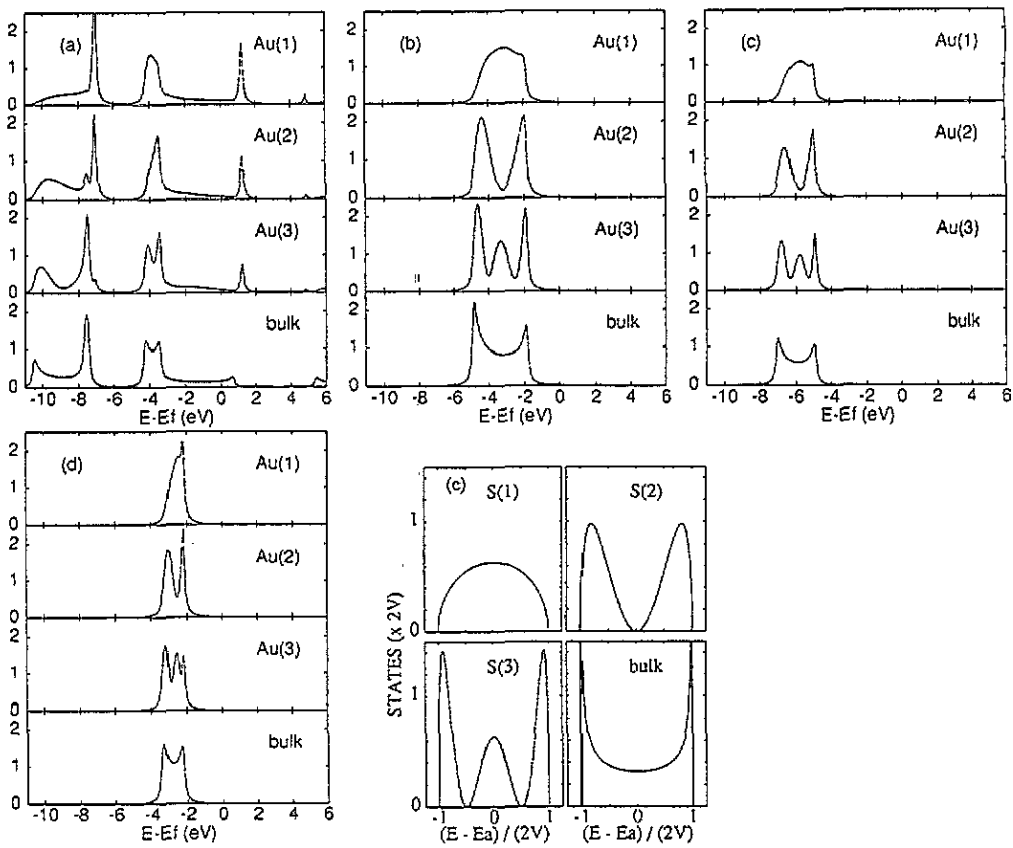

Figure 5. Layer-resolved Au–1 × 1 surface density of states at the centre of the surface Brillouin zone: (*a*) Δ_1; (*b*) Δ_5; (*c*) Δ_2; (*d*) $\Delta_{2'}$ states; (*e*) site-projected density of states for a semi-infinite one-level tight-binding chain. $S(n)$ is the nth site from the chain end, E_A is the atomic level and V the nearest-neighbour hopping. The small feature at 4.85 eV in (*a*) is the barrier state corresponding to the $n = 1$ image state of the Au surface.

matched. Comparison of the Fe ΓH and Au ΓX band structures indicate that in this limit the $\Delta_2^{\uparrow\downarrow}$, $\Delta_{2'}^{\uparrow\downarrow}$ and $\Delta_5^{\downarrow}$ Fe and Au states do not line up. Consequently, Fe states of these symmetries within the thin film will be confined. If this behaviour persists in thinner films (i.e. if the Fe–Au interaction is weak), the Fe states will form quantum well (QW) states. Calculation of the $\bar{\Gamma}$ DOS indicates that this picture is valid right down to the monolayer limit. As an illustration, the Δ_2 states for $Au_1Fe_3Au_\infty$ are shown in figure 6. On the Au layers on the substrate side the DOSs again resemble those of the semi-infinite TB model (2), forming a continuum of essentially spin-degenerate states whose profile picks up an additional peak for each layer away from the interface. Directly at the interface, the Au(1) profile indicates a large downward shift in the states consistent with the behaviour observed in the core levels, whilst on the Au overlayer a single sharp peak exists coincident with the bulk continuum, with only a very small spin splitting. In contrast, the Fe states are split by some 2 eV and form a series of discrete levels, one for each Fe layer (in this case three). Rather surprisingly, the central Fe layer only exhibits two states for each spin direction. To understand this, we again consider a one-band TB chain, this time of finite length with sites

$1, 2, \ldots, n$. The resulting spectrum of states and the corresponding eigenfunctions may be obtained by direct diagonalization—for $n = 3$ these are

$$E = E_A + \sqrt{2}V \qquad |\psi\rangle = \tfrac{1}{2}\left(|1\rangle - \sqrt{2}|2\rangle + |3\rangle\right)$$

$$E = E_A \qquad |\psi\rangle = \tfrac{1}{2}\left(\sqrt{2}|1\rangle - \sqrt{2}|3\rangle\right)$$

$$E = E_A - \sqrt{2}V \qquad |\psi\rangle = \tfrac{1}{2}\left(|1\rangle + \sqrt{2}|2\rangle + |3\rangle\right). \tag{3}$$

The eigenvalues are equally spaced. The charge density $\langle\psi|\psi\rangle$ corresponding to the middle eigenvalue has zero weight on the central site, whilst the weight on the outer sites for three states are in the ratio 1:2:1. These are exactly the features of the full calculation, figure 6. Extending this analysis to other Fe film thicknesses we can monitor the development of the Fe states with film thickness by recording the position of these discrete states as a function of n. These are shown in figure 7 for the Δ_2, $\Delta_{2'}$ and Δ_5 states. In some cases, notably $\Delta_{2'}^{\uparrow\downarrow}$ and $\Delta_5^{\downarrow}$, the similarity with the simple model is remarkable—these are the states which most closely resemble a one-dimensional TB band within the Fe bulk *and* which are separated from the corresponding Au levels. For $\Delta_2^{\uparrow\downarrow}$ states the discrete states are more dense at the lower energies, mimicking the bulk distribution. In the case of the $\Delta_5^{\uparrow}$ states the Au and Fe states partially overlap in energy and the ideal distribution is again modified.

More difficult to interpret are states of Δ_1 symmetry. These couple strongly to the surface potential, the respective Au and Fe bulk bands have more complicated dispersion and in large regions coexist in energy, figure 8. Consequently electrons in some Fe levels within the film are not confined but resonant with substrate levels and the level width is increased. The Δ_1 layer-resolved DOS for the three narrowest Fe films are shown in figure 9. The differences between the profiles of the substrate Au layers here, and those of the clean surface, figure 5, reflect the different termination (vacuum versus Fe layers, into which electrons can tunnel at some energies). On the Au overlayer, the broad hump at -8 eV in figure 9(a) is a state predominantly localized on the surface Au layer. With increasing Fe film thickness this level sharpens and moves down to -8.5 eV, approximately the centre of the lowest bulk Au Δ_1 band to which it corresponds. The state decays over 3–4 Fe layers and hence the broad width for $n = 1$ when the electrons couple strongly to the Au substrate across the Fe film. The sharp peak at -6.5 eV in figure 9(a) is an Fe-derived state. It is replaced by two states in figure 9(b) and three in figure 9(c), behaviour similar to that previously noted. For greater Fe coverages the widening distribution of states places some levels outside the substrate band gap, extending from ~ -7.5 eV to ~ -4.5 eV (figure 8), and these states are less well resolved. For $n = 10$ five Fe QW states lie within the gap. Interestingly, these states have considerable weight on the interface Au layers but are absent from the Au(2) layer. Their splitting is small, closer to that of the bulk Γ_1 states than those higher in energy. In the thin films the states lie slightly lower in energy than would be predicted from the bulk Fe band structure—this is due to the lower Fe potential, as seen in the core level shifts. In figures 9(b) and 9(c) the spin-split pair of states at -2.7 eV($\uparrow$) and -1.8 eV($\downarrow$) correspond to the bulk Au bands which lie between -4.3 and $+0.7$ eV. The exchange splitting arises from the large overlap with states on the neighbouring Fe layer, and corresponding peaks may be seen on the Fe(1) layer. In the monolayer this interaction enables the electrons to tunnel through into the substrate and the sharp state is replaced by a broad band. The overlap with states in the Fe(2) layer is much smaller, so for the bilayer and thicker films the states are sharp.

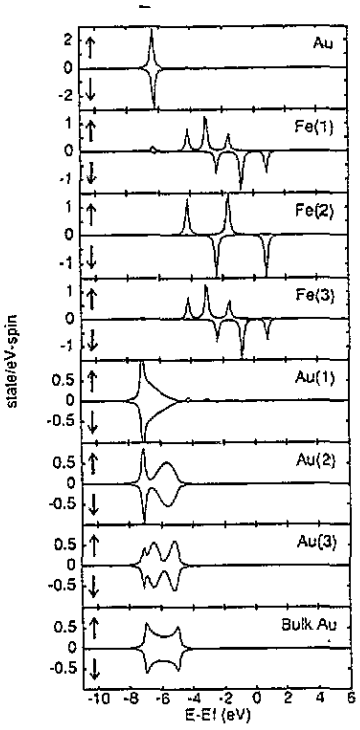

Figure 6. Spin-resolved layer-projected density of states of Δ_2 symmetry at $\bar{\Gamma}$ for $Au_1Fe_3Au_\infty$.

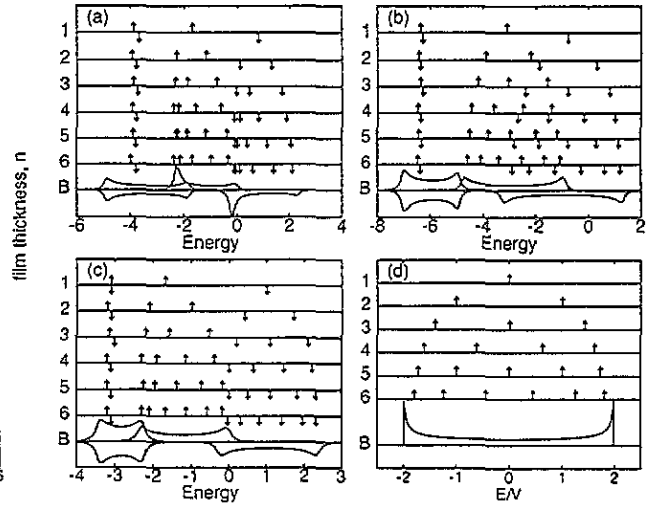

Figure 7. Distribution of quantum well states in $Au_1Fe_nAu_\infty$ for $1 \leqslant n \leqslant 6$. States of (*a*) Δ_2, (*b*) $\Delta_{2'}$ and (*c*) Δ_5 symmetry are shown, spin resolved, along with the Au and Fe continuum of states for the $n \rightarrow \infty$ limit. The Au overlayer states are also plotted. In (*d*) the distributions of states within the one band tight-binding linear chain model are also shown.

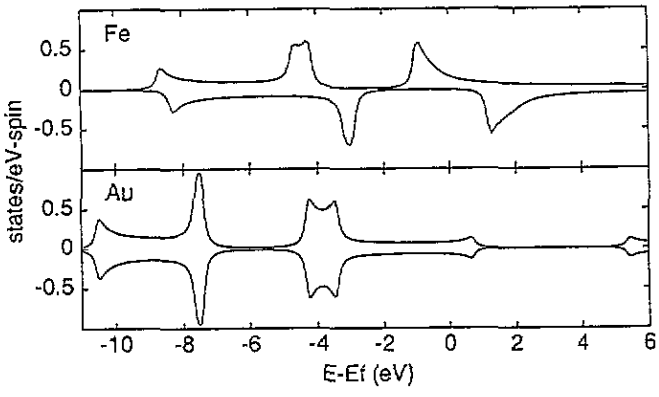

Figure 8. Density of states of Δ_1 symmetry arising from states in the bulk ΓH (Fe) and ΓX (Au) directions.

The second bulk Fe Δ_1 bands (figure 8) extend between $-1.0(\uparrow)/+1.2(\downarrow)$ eV and approximately +9.5 eV, and have a fairly straightforward TB profile; for the thin films, this would imply a series of QW states centred around +4.5 eV(↑) and +5.5 eV(↓). No such states are to be seen. With a substrate band with lower band edge just below 6 eV and the vacuum level around 5 eV, many of the QW states would be able to couple to substrate and vacuum states, and hence be broadened into resonances. However, no such resonances are to be seen either, except in film thicknesses $n > 5$. Instead, strong interaction between Fe

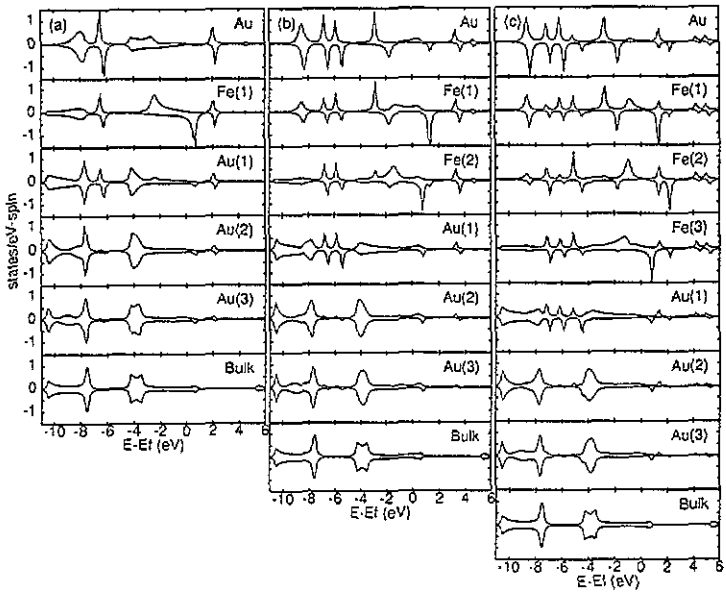

Figure 9. Δ_1 symmetry layer-projected density of states for (*a*) $n = 1$, (*b*) $n = 2$ and (*c*) $n = 3$ $Au_1Fe_nAu_\infty$ overlayer thin films.

and Au states lowers the Fe states in the thinner films by several volts. Thus, in figure 9(*a*), there is a Fe majority peak at -2.5 eV, mixing strongly with the Au overlayer state, and a minority state at $+0.7$ eV. An almost spin-degenerate state at $+2.0$ eV is also visible. (This state is *not* a surface state since it also exists in the $Au_\infty Fe_1 Au_\infty$ sandwich. It has been seen in inverse photoemission (Himpsel 1991).) In the $n = 2$ film majority states are found at -2.8 eV, -1.3 eV, $+0.4$ eV and $+3.3$ eV, and minority states at -1.8 eV, $+0.8$ eV, $+1.3$ eV and $+3.6$ eV. States corresponding to the highest of these levels also exists in the $Au_\infty Fe_2 Au_\infty$ sandwich.

7. Summary

Systematic studies of the development of thin-film electronic and magnetic properties with film thickness have been presented, focusing on the Fe/Au(001) system. Work function, core level shifts and band narrowing of the clean Au surface are in excellent agreement with experiment, indicating that the clean metal surface is well described by the computational scheme employed. For the thin film, calculated work function changes are consistent with measured image state variations, and magnetic moments and core-level shifts agree with the results of more elaborate calculations where available.

The properties of the Fe film show interfacial features which decay to bulk-like behaviour over various lengths. Most local are the core-level shifts, which vary only with the nearest-neighbour environment and so are specific to the interfacial planes. The shifts indicate a lowering of the interface potential, which is also to be seen in the density of states and the one-electron energy levels. The Fe and Au densities of states are dominated by d electron contributions and the profiles also reflect nearest-neighbour changes, although on the scale of the sp contributions the perturbations extend many planes from the interface.

Magnetic moments are enhanced within three layers of the interface. These show little asymmetry despite the asymmetry in the sandwiching half-spaces—an Au substrate and a Au monolayer. The hyperfine fields within the film show a strong finite-size effect; in thicker films, the largest shift (relative to bulk Fe) arises from the Fe layer one layer away from the interface (Fe(2), Fe($n-1$) in the n-layer film). A positive valence contribution on the interfacial Fe layer compensates the larger negative core contribution due to the greatly enhanced moment.

These calculations incorporate truly semi-infinite substrates, and hence the correct description of continuum states, allowing unambiguous identification of localized states and resonances. There is no screening on the level of individual electron states, which show behaviour characteristic of the thin-film geometry even up to 10 Fe layers. At the Brillouin zone centre, with the exception of states of Δ_1 symmetry (scalar-relativistic treatment) a simple picture emerges with Fe states confined by substrate band gaps and the vacuum barrier, forming a discrete spectrum of quantum well states whose positions are largely governed by the corresponding bulk Fe band structure. The Δ_1 states are less well confined—at lower energies many Fe states tunnel into the Au substrate whilst higher states mix strongly with the Au levels and are shifted down considerably in energy. These effects prevent the simple analysis of the quantum well states, which is potentially important for the discussion of magnetic coupling in magnetic superlattices (Ortega and Himpsel 1992). In addition, Loly and Pendry (1983) have proposed the use of metallic thin-film states as a means of accurate band structure determination by photoemission. As seen in the states of Δ_2, $\Delta_{2'}$ and Δ_5 symmetry, the positions of the quantized states reflect the bulk band structure and will give rise to structure in the photocurrent which can be measured. The behaviour of the Δ_1 symmetry states here indicate that a simple analysis is not always possible, even with a transition-metal/noble-metal system. In particular, the potential shift seen in core levels should be taken into account, and even cases where these are not seen may require fully self-consistent calculations. More work is required to determine this. In this regard, the present calculations can be improved by a more accurate treatment of the crystal potential permitting the inclusion of interlayer relaxation. New techniques enabling this are being developed (Crampin *et al* 1992). Spin–orbit coupling must also be treated to enable realistic comparison with experiment.

Acknowledgment

This work is supported by the Stichting voor Fundamenteel Onderzoek der Materie.

Appendix. One-band tight-binding linear chain

Starting with a chain of identical sites, spacing a, labelled by site index n, $(-N < n < N)$, with on-site energies E_A and nearest-neighbour hopping V, we have the Hamiltonian

$$H_0 = \sum_n |n\rangle E_A \langle n| + V \sum_n (|n\rangle\langle n+1| + |n\rangle\langle n-1|). \tag{A1}$$

We assume orthonormal orbitals: $\langle n|m\rangle = \delta_{nm}$. The resulting eigenstates $|k)$ and eigenvalues E_k are

$$|k) = \frac{1}{\sqrt{2N+1}} \sum_n e^{ikan} |n) \qquad E_k = E_A + 2V\cos(ka). \tag{A2}$$

In the limit $N \to \infty$, the Green function for energies within the continuum, $|E| < 2V$, is readily shown to be

$$\langle n|G_0^+(E)|m\rangle = \sum_k \frac{\langle n|k\rangle\langle k|m\rangle}{E + i0 - E_k} = \frac{-ie^{-i|n-m|\Theta}}{2V \sin\Theta} \tag{A3}$$

with $\Theta = \cos^{-1}[(E - E_A)/2V]$. Introducing an impurity at site 0, with level $E_A + \Delta$, we have

$$H = H_0 + H_i \qquad H_i = |0\rangle\Delta\langle 0| \tag{A4}$$

and so from the Dyson equation we obtain the new Green function

$$\langle n|G^+(E)|m\rangle = \langle n|G_0^+(E)|m\rangle + \langle n|G_0^+(E)|0\rangle\Delta\langle 0|G_0^+(E)|m\rangle/[1 - \Delta\langle 0|G_0^+(E)|0\rangle]. \tag{A5}$$

Taking the limit $\Delta \to \infty$, the two semi-infinite chains to either side of site 0 become decoupled, creating two identical surfaces. The site-projected density of states is then

$$\rho_n(E) = -(1/\pi)\mathrm{Im}\langle n|G^+(E)|n\rangle = (\sin^2|n|\Theta)/\pi V \sin\Theta. \tag{A6}$$

References

Bader S D and Moog E R 1987 *J. Appl. Phys.* **61** 3729–34
Bader S D, Moog E R and Grünberg P 1986 *J. Magn. Magn. Mater.* **53** L295–8
von Barth U and Hedin L 1972 *J. Phys. C: Solid State Phys.* **5** 1629–43
Besocke K, Krahl-Urban B and Wagner H 1977 *Surf. Sci.* **68** 39–46
Citrin O H, Wertheim G K and Baer Y 1978 *Phys. Rev. Lett.* **41** 1425–8
Crampin S 1991 unpublished
Crampin S, Hampel K, Vvedensky D D and MacLaren J M 1990 *J. Mater. Res.* **5** 2107–19
Crampin S, van Hoof J B A N, Nekovee M and Inglesfield J E 1992 *J. Phys.: Condens. Matter* **4** 1475–88
Drittler B, Weinert M, Zeller R and Dederichs P H 1989 *Phys. Rev.* B **39** 930–9
Dürr W, Taborelli M, Paul O, Germat R, Gudat W, Pescia D and Landolt M 1989 *Phys. Rev. Lett.* **62** 206–9
Eckardt H, Fritsche L and Noffke J 1984 *J. Phys. F: Met. Phys.* **14** 97–121
Freeman A J and Fu C L 1987 *J. Appl. Phys.* **61** 3356–61
Fu C L and Freeman A J 1987 *Phys. Rev.* B **35** 925–32
Fuss A, Demokritov S, Grünberg P and Zinn W 1992 *J. Magn. Magn. Mater.* **103** L221–7
Hansson G V and Flodström S A 1978 *Phys. Rev.* B **18** 1572–89
Heinen W, Carbone C, Kachel T and Gudat W, 1990 *J. Electron Spectrosc. Relat. Phenom.* **51** 701–12
Himpsel F J 1991 *Phys. Rev.* B **44** 5966–9
Himpsel F J and Ortega J E 1992 *Phys. Rev.* B **46** 9719–23
Hölzl J and Schulte F K 1979 *Solid Surface Physics* (Berlin: Springer)
Inglesfield J E 1978 *Surf. Sci.* **76** 355–78
Jepson O, Glötzel D and Mackintosh A R 1981 *Phys. Rev.* B **23** 2684–96
Knab D and Koenig C 1991 *Phys. Rev.* B **43** 8370–8
Koelling D D and Harmon B N 1977 *J. Phys. C: Solid State Phys.* **10** 3107–14
Korecki J and Gradmann U 1985 *Phys. Rev. Lett.* **55** 2491–4
Li C, Freeman A J and Fu C L 1988 *J. Magn. Magn. Mater.* **75** 201–8
Loly P D and Pendry J B 1983 *J. Phys. C: Solid State Phys.* **16** 423–31
MacLaren J M, Crampin S, Vvedensky D D and Pendry J B 1989 *Phys. Rev.* B **40** 12 164–75
Maurer M *et al* 1991 *J. Magn. Magn. Mater.* **93** 15–24

Mokrani A, Demangeat C and Dreyssé H 1990 *Phys. Rev.* B **42** 8670–2
Moruzzi V L, Janak J F and Williams A R 1978 *Calculated Electronic Properties of Metals* (New York: Pergamon)
Noffke J and Fritsche L 1981 *J. Phys. C: Solid State Phys.* **14** 89–95
Ohnishi S, Freeman A J and Weinert M 1983 *Phys. Rev.* B **28** 6741–8
Ohnishi S, Weinert M and Freeman A J 1984 *Phys. Rev.* B **30** 36–43
Ortega J E and Himpsel F J 1992 *Phys. Rev. Lett.* **69** 844–7
Shinto T, Araki S and Hosoito N 1990 *J. Magn. Magn. Mater.* **90–1** 753–7
Skriver H L and Rosengaard N M 1991 *Phys. Rev.* B **43** 9538–49